Analytical representation of the swirling flow upstream the Kaplan turbine runner for variable guide vane opening

Sebastian MUNTEAN* Romanian Academy Timisoara Branch, Romania
seby@acad-tim.tm.edu.ro
Daniel BALINT Politehnica University of Timisoara, Romania
balint@acad-tim.tm.edu.ro
Romeo SUSAN- RESIGA Politehnica University of Timisoara, Romania
resiga@mh.mec.upt.ro
Sandor BERNAD Romanian Academy Timisoara Branch, Romania
sbernad@mh.mec.upt.ro
Ioan ANTON Politehnica University of Timisoara, Romania
anton@acad-tim.tm.edu.ro

Key words: analytical representation of swirling flow, Kaplan turbine, 3D numerical investigation

Abstract

In order to improve both the efficiency and cavitational behaviour of the Kaplan turbine, the velocity field upstream to the runner is analyzed. The spiral case and distributor generate a suitable swirling flow further ingested by the Kaplan runner. An important step in designing and/or optimizing the runner blades is the determination of both axial and tangential velocity components at runner inlet. The radial distribution of both tangential (c_u) and axial (c_a) velocity coefficients on the annular section upstream the runner blades are presented. Traditionally, the analytical expression considered for c_u corresponds to a free vortex, while c_a is considered constant. However, these design assumptions are quite far from the actual velocity field, particularly as the turbine guide vane opening is decreased. An original analytical representation of the swirling flow in a section just upstream the runner blades is proposed, and it is shown to fit almost perfectly the numerical data. This conclusion is important in the framework of hydraulic turbines refurbishment, as well as for design optimization.

Introduction

The hydrodynamics of Kaplan turbines is a more than a century old subject that benefits from a large body of both theoretical and experimental investigations (Ref 1, Ref 2). Traditionally,

the main subject of these studies has been the turbine runner, with the development of powerful and reliable tools for designing the runner blades. Simplified quasi-3D methods are currently used in the runner domain, taking advantage on the quasi-axial meridional flow in this region. Also, a practical combined method of the circumferentially averaged mean through-flow is developed and applied to the case of Kaplan turbine by Peng (Ref 3). On the other hand, the spiral case, distributor (stay vanes and guide vanes), as well as the draft tube, do not lend themselves to such a simplified analysis due to the intrinsic three-dimensionality of the flow. As a result, a realistic analysis of the spiral case/distributor hydrodynamics must consider a full 3D flow simulation. This is the approach employed by most of recent studies that use numerical simulations (Ref 4 – Ref 6). On the other hand, the flow upstream the turbine runner can be considered steady. As a result, a 3D steady flow model is employed in the present study.

The main purpose of the spiral case and distributor is to prepare a suitable swirling flow further ingested by the Kaplan runner. An important step in designing and/or optimizing the runner blades is the determination of both axial and tangential velocity components at runner inlet. Traditionally, the analytical expression considered for tangential velocity component c_u corresponds to a free vortex, while axial velocity component c_a is considered constant. However, these design assumptions may be quite far from the actual velocity field. As a result, we have introduced a new analytical representation of the velocity components upstream to the Kaplan runner at best efficient point (Ref 6).

The energetical and cavitational behaviors of the Kaplan runner at off-design operating points represent an essential issue. Consequently, the velocity profile downstream to the distributor at off-design operating conditions is needed. Since we are not interested in modeling the perturbations produced by the stay and guide vane wakes, we are performing in the present paper an inviscid 3D steady flow numerical simulation. The 3D incompressible Euler flow is computed using the commercial expert code FLUENT 6.0.12 (Ref 7). Moreover, according to the IEC 60193 Standard (Ref 8), the characteristic Reynolds number of the prototype hydraulic turbine is larger than 10^7, supporting the Euler simulation.

Section 2 presents the computational domain for a real Kaplan spiral case and distributor. The outflow section is conventionally defined as the Kaplan turbine runner reference plane. A 3D structured mesh is generated, with approximately 2×10^6 finite volume cells (Ref 9). This section also presents the inflow/outflow boundary conditions considered in the present study.

Section 3 is devoted to the flow numerical simulation and analysis of the 3D hydrodynamic field for the 6 operating points considered at constant head and variable guide vane opening, together with the analysis of the swirling flow upstream the Kaplan runner.

The last section presents the main conclusions of the present study as well as its relevance to the Kaplan turbine design and optimization.

Computational domain. Equations and boundary conditions

Figure 1 (left) presents the cross section through the Kaplan turbine as well as the computational domain considered in the present study. The inlet section of computational domain corresponds to the power plant inlet section. Figure 1 (right) shows the 3D computational domain considered in the present study.

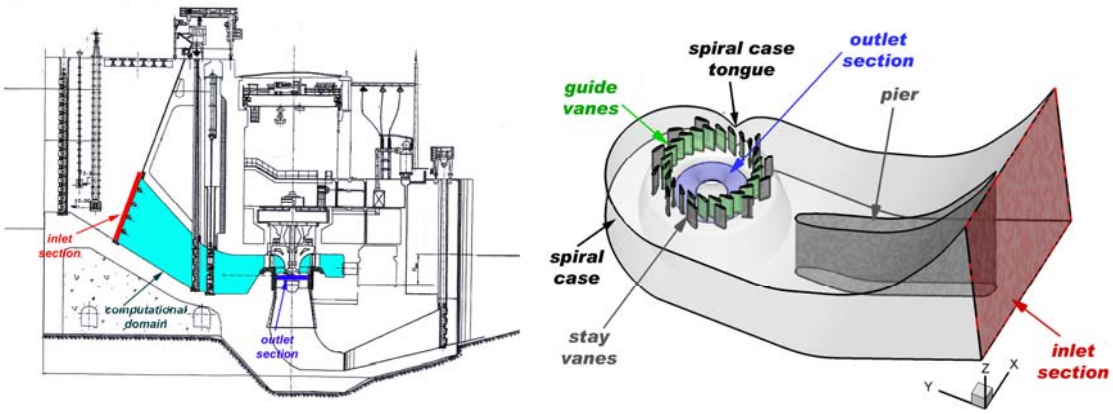

Figure 1 3D computational domain extends from the power plant inlet to the runner reference plane.

The stay vanes have different profiles, as shown in Figure 2. The first seven (1 … 7) stay vanes are identical, followed by a different vane 8, two identical vanes 9 and 10, and finally a different stay vane 11 near the spiral case tongue. All 24 guide vanes are identical and have a symmetrical profile, as shown in Figure 2.

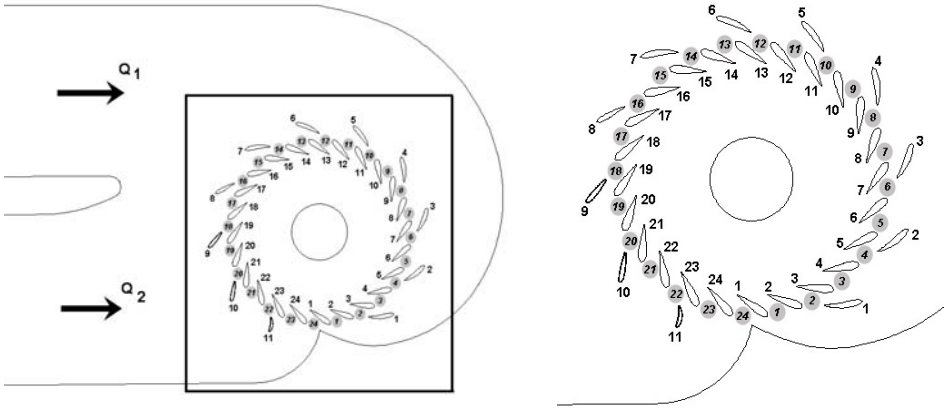

Figure 2 Top view of the spiral case and distributor (left) and a detail view of the stay and guide vanes (right).

The oulet section is conventionally chosen at the runner reference plane. Normally, one would consider a computational procedure that couples the steady absolute flow in spiral case/distributor domain with the relative flow in the runner (Ref 10). However, a separate flow simulation can still be performed in the domain from Figure 1 (left), by choosing a

suitable boundary condition on the outlet section.

An structured 3D mesh is generated. In the inflow region we consider a relatively coarse mesh, and the mesh is further refined downstream as the flow accelerates. A particular attention is paid to the discretization near the stay/guide vanes, to correctly represent the local large velocity gradients. The mesh has approximately 2 million computational cells.

A 3D steady, inviscid and incompressible flow is considered, thus we solve the steady Euler equations:

$$\nabla \cdot \mathbf{V} = 0 \qquad (1)$$

$$\rho\left(\mathbf{V} \cdot \nabla\right)\mathbf{V} = -\nabla p \qquad (2)$$

On the inlet section we prescribe a constant total pressure. The value of the total pressure is adjusted to obtain the maximum operating flow rate for the Kaplan turbine under consideration. On the outlet section, the swirling flow structure is compatible with the so-called pressure radial equilibrium. This condition is derived from the radial component of the Euler equation,

$$V_r \frac{\partial V_r}{\partial r} + \frac{V_u}{r}\frac{\partial V_r}{\partial \theta} + V_z \frac{\partial V_r}{\partial z} - \frac{V_u^2}{r} = -\frac{1}{\rho}\frac{\partial p}{\partial r} \qquad (3)$$

If the radial velocity component is negligible, $V_r \approx 0$, one obtains the pressure radial equilibrium condition,

$$\frac{1}{\rho}\frac{\partial p}{\partial r} = \frac{V_u^2}{r} \qquad (4)$$

This condition has been successfully employed on the draft tube inlet section when computing the runner flow (Ref 11), and it has been validated experimentally (Ref 12). A reference pressure is conventionally set to zero at the hub on the outlet section, since condition (4) defines the pressure only up to an additive constant.

Note that (4) does not actually takes into account the runner influence on the flow upstream, but we consider it appropriate for evaluating the performance of the spiral case and distributor. The rest of the domain boundary corresponds to solid walls, with zero normal velocity condition.

The computations have been performed in six operating points, see Figure 3. The parameters of the operating points investigated are presented in Table 1.

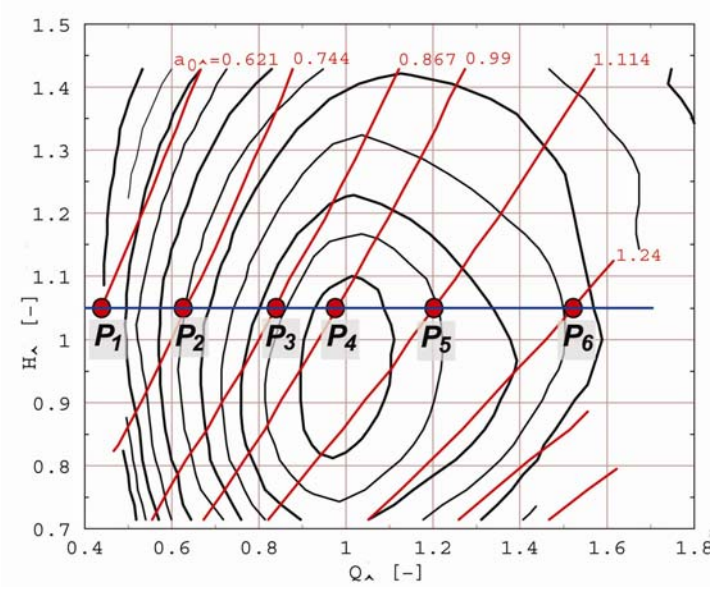

Figure 3 Kaplan turbine hill chart and the operating points investigated.

Table 1 Parameters for the operating points investigated.

Operating Point	$H^{\wedge}$	$Q^{\wedge}$	$a_{0^{\wedge}}$
P_1		*0.4589*	*0.621*
P_2		*0.6453*	*0.744*
P_3	*1.05*	*0.8442*	*0.867*
P_4		*0.9767*	*0.990*
P_5		*1.2000*	*1.114*
P_6		*1.5139*	*1.240*

Analytical Representation of Axial and Tangential Velocity Profiles upstream the Kaplan Runner

As mentioned before, the spiral case and distributor generate a suitable swirling flow further ingested by the Kaplan runner. An important step in designing and/or optimizing the runner blades is the determination of both axial and tangential velocity components upstream the Kaplan runner. Consequently, the hydrodynamic field in an annular section displaced at $0.2\,R_{\text{ref}}$ upstream the reference plane of runner is investigated. In order to generate a parametric description of both tangential and axial velocity components upstream to the Kaplan runner an original analytical representation of the swirling flow is developed by Susan-Resiga et al. (Ref 13) and applied to the flow field upstream to the Kaplan runner at best efficiency point, (Ref 6).

Several swirling flow models have been developed in the literature to study the vortex flow. The distribution of the tangential velocity in a real swirling flow is mainly due to the method

used to generate the swirl. From a mathematical point of view, it is possible to create models to properly approximate the behavior of the flow field. A Rankine vortex represents a simply model for rotating flow (see Figure 4). It displays a solid body rotation core followed by a r^{-1} decay in the radial direction corresponding to a free vortex. In application to a swirling flow, it is worth to note that the model does not take into account the finite thickness of the shear layer region at $r = R_c$ where the curve has an angular point, Figure 4. The characteristic vortex radius R_c measures the vortex core radial extent (see the grey region marked in Figure 4). These two parameters define the Rankine vortex tangential velocity,

$$c_u(r) = \begin{cases} \Omega r \ , \ 0 \le r \le R_c \\ \dfrac{\Omega R_c}{r} \ , \ r \ge R_c \end{cases} \qquad (5)$$

where r is the radial distance from the vortex axis. This simplified model provides a continuous function for $c_u(r)$, but the derivative is discontinuous.

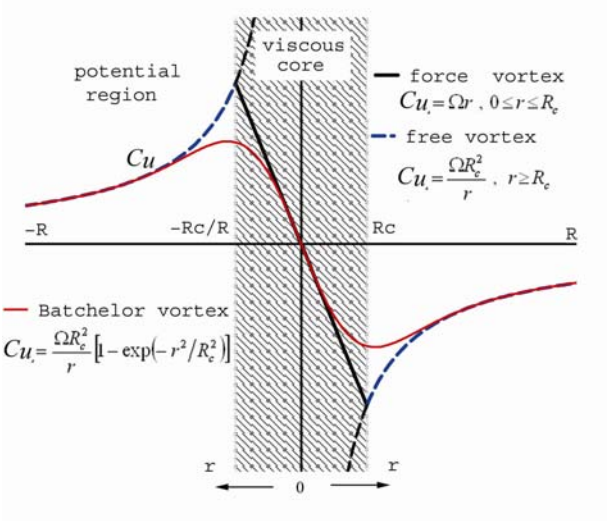

Figure 4 The models of tangential velocity distribution in swirling flow.

A more suitable model for developed swirling flows is the Batchelor vortex (solid line in Figure 4). The tangential velocity field is described via a similarity solution applied to wakes in the far field:

$$c_u(r) = \frac{\Omega R_c^2}{r}\left[1 - \exp\left(-\frac{r^2}{R_c^2}\right)\right] \qquad (6)$$

As a result, we introduce in this paper a new analytical representation of the velocity components as

$$c_u = \Omega_0 r + \Omega_1 \frac{R_1^2}{r}\left[1 - \exp\left(-\frac{r^2}{R_1^2}\right)\right] + \frac{\Gamma}{r}, \qquad (7a)$$

$$c_z = V_0 + V_1 \exp\left(-\frac{r^2}{R_1^2}\right) + V_2 \frac{r}{R_{ref}}. \qquad (7b)$$

The last term in Eq. (7a) has been added in agreement with the constant used by Dahlhaug (Ref 12) for representing $c_u(r)$. The velocity coefficients are defined as $c = V/U_{ref}$. The same normalization is considered for the characteristic velocities V_0, V_1 and V_2 in Eq. (7b). The characteristic angular velocities Ω_0, Ω_1 in Eq. (7a) are normalized by Ω, Γ by ΩR_{ref}^2, while the radius r and the characteristic radii R_1, R_2 are normalized with the reference radius R_{ref}. Eqs. (7) corresponds to a superposition of one solid body vortex, one Batchelor vortex (Ref 14) and one free vortex, (Ref 15). The particular expression of an elementary vortex,

$$c_u = \Omega \frac{R^2}{r}\left[1 - \exp\left(-\frac{r^2}{R^2}\right)\right] \qquad (8a)$$

$$c_z = V \exp\left(-\frac{r^2}{R^2}\right) \qquad (8b)$$

has been successfully used by Faler and Leibovich (Ref 16) to describe the swirl structure generated by a radial vane apparatus. Note that if the vortex characteristic radius R_c goes to infinity, the Batchelor vortex Eqs. (8) becomes a pure forced vortex:

$$c_u = \Omega r \qquad (9a)$$

$$c_z = V \qquad (9a)$$

A special least-square procedure has been developed by the authors to fit Eqs. (7) with numerical data. The first forced vortex has a dimensionless angular velocity Ω_0 and an associated constant axial velocity V_0. The second vortex, of Batchelor type, is co-rotating with the first vortex, Ω_1, and has a characteristic radius R_1. The second vortex is counter-flowing with respect to the first one, V_1. The third is a free vortex.

Table 2 Fit parameters of axial and tangential velocity components for operating points.

OP	Ω_0	V_0	R_1	Ω_1	V_1	Γ	V_2/R_{ref}
P_1	-0.035110	-0.278091	0.2772	12.759	1.2923	-0.7827	0.218939
P_2	0.063804	-0.262482	0.1857	177.465	11.847	-6.1080	0.149239
P_3	0.065119	-0.262984	0.1378	2354.01	57.7044	-44.5086	0.113895
P_4	0.078983	-0.292984	0.1393	1723.33	63.0590	-33.2816	0.111705
P_5	0.099701	-0.341409	0.1406	1147.77	73.3568	-22.5286	0.105257
P_6	0.128013	-0.405412	0.1434	689.65	69.5708	-14.0217	0.093206

Figures 4 show the radial distribution of the radial (*cr* denoted with black circles ○), tangential (*cu* labeled with red squares □) and axial (*cz* plotted with green triangles ▵)

velocity coefficients on the annular section upstream the runner blades for all operating points as well as the curves fitted with Eqs. (7a) and (7b) (black solid lines). The velocity coefficients are negative because the axial velocity component is negative in the coordinate system from Fig. 5.

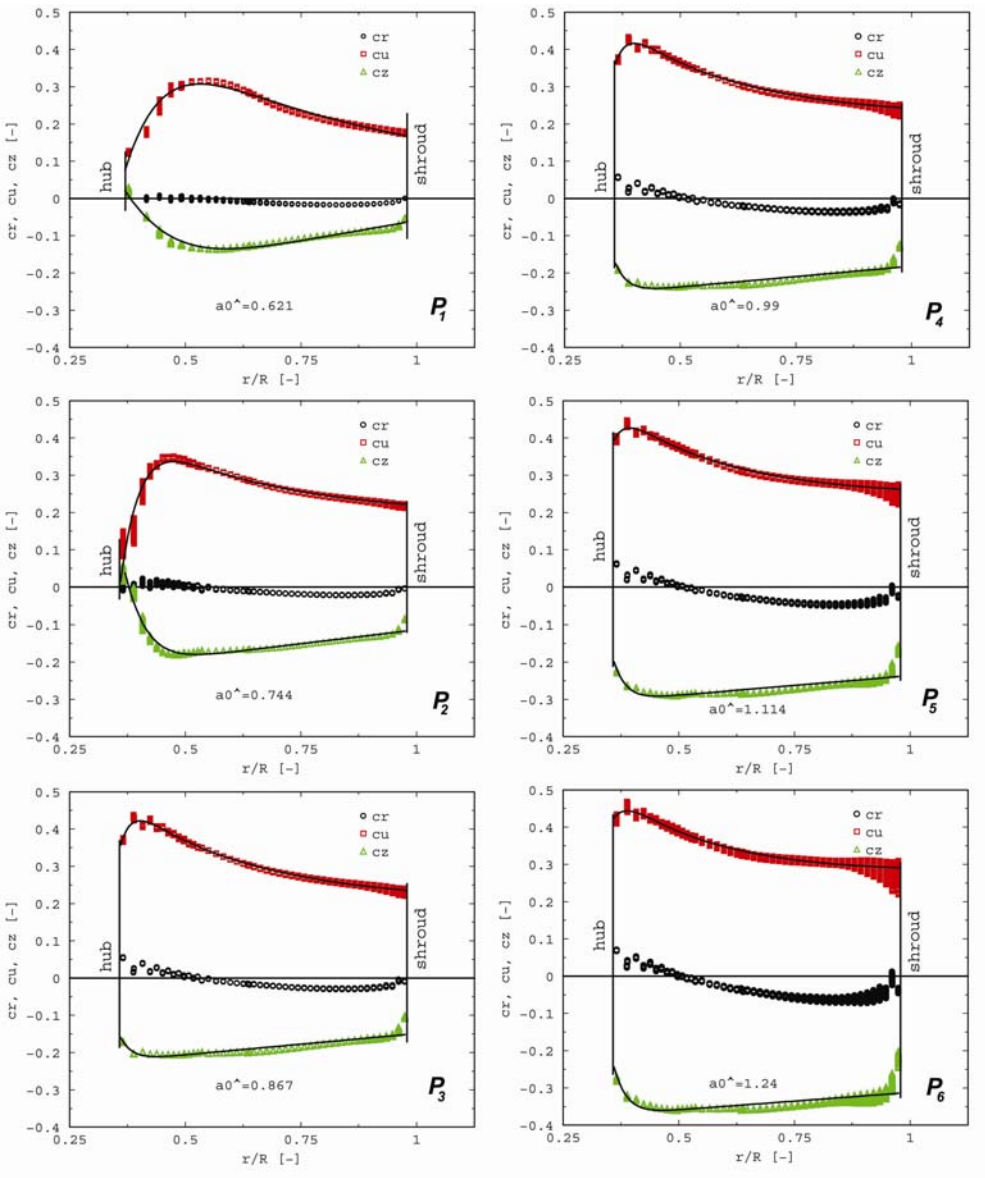

Figure 5 The velocity coefficients versus dimensionless radius upstream the Kaplan runner for operating points investigated.

A significant modification of the tangential and axial velocity coefficients are obtained at operating points P_1 and P_2. Figure 6 presents the axial velocity coeficient versus dimensionless radius for all points investigated. One can observe at operating points P_1 and P_2 the axial velocity is positive near the hub. Consequently, a recirculation region is generated at high intensity of the swirl.

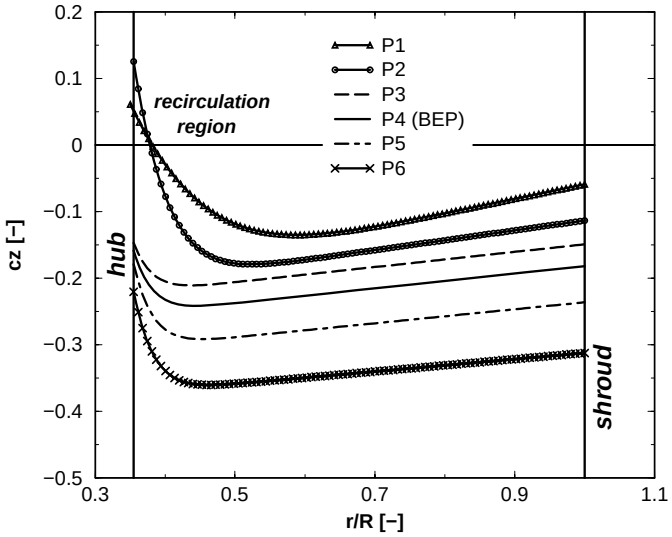

Figure 6. The distribution of the axial velocity coefficient versus dimensionless radius upstream the Kaplan runner for operating points.

Ploting the characteristic velocity V_0 from Table 2 in terms of the dimensionless guide vane opening it is found the boundary between two domains, see Figure 7. The minimum magnitude of V_0 is reached at dimensionless guide vane opening 0.777 ($a_{0^\wedge} \approx 0.8$). Accordingly, velocity profiles start to modify when the dimensionless guide vane opening smaller than 0.8 ($a_{0^\wedge} < 0.8$).

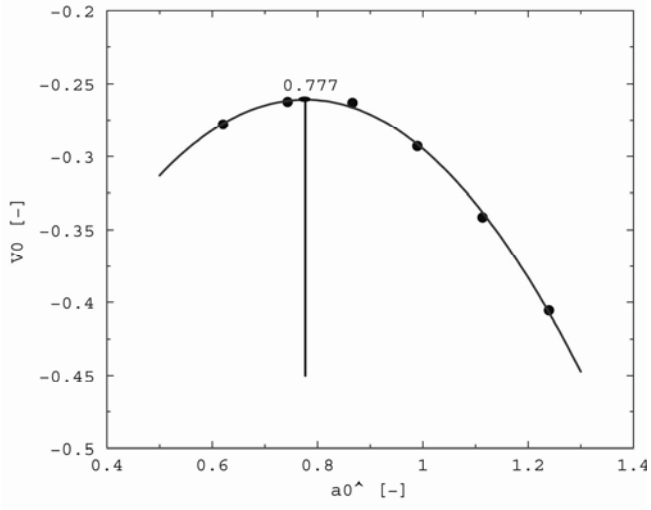

Figure 7. The distribution of the characteristic velocity of solid body vortex versus dimensionless guide vane opening.

Figure 8 shows the tangential velocity coeficient in terms of the dimensionless radius. The same conclusion emerges from tangential profiles like axial profiles when dimensionless

guide vane is smaller then $a_{0_\wedge} < 0.8$. Moreover, one can see all tangential velocity profiles present a transition region from solid body vortex to free vortex near the hub. It means that the hub radius is chosen too small. Unfortunately, this situation induces hydrodynamics instabilities when the hydraulic turbine operates at partial loading.

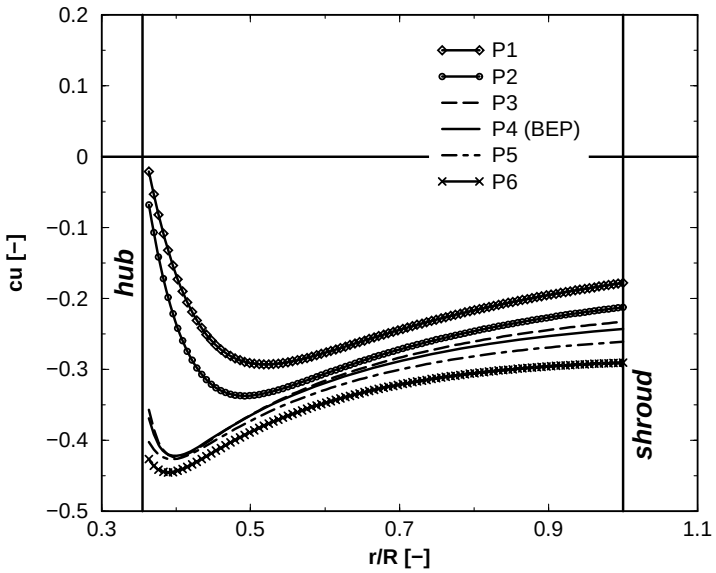

Figure 8. The distribution of the tangential velocity coefficient versus dimensionless radius upstream the Kaplan runner for operating points.

A global quantitative of the incompressible swirling flow is provided by the swirl number *S* as the axial momentum divided by the axial flux of axial momentum.

$$S = \frac{\int_{R_h}^{R_s} r^2 V_z V_u \, dr}{R_s \int_{R_h}^{R_s} r V_z^2 \, dr} \qquad (10)$$

The swirl number computed for the swirling flow given by Eq. (10) is plotted versus the dimensionless guide vane opening, Figure 9. One can see that for the investigated range of the swirl number decreases as the dimensionless guide vane opening increases, but nevertheless the variation is quasi-linear.

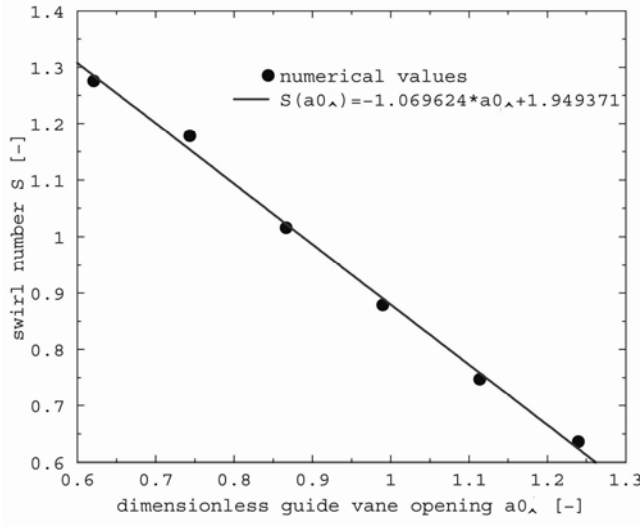

Figure 9. The swirl number versus dimensionless guide vane opening.

Conclusions

The paper presents a methodology for computing the full three-dimensional flow upstream the Kaplan turbine runner. We have developed a methodology for accurately describing the complex 3D geometry, as well as for building a suitable structured 3D mesh. A significant step forward has been made to reduce the time devoted to the problem definition (geometry and mesh), in order to be able to apply the present approach for design improvement and optimization.

The velocity component profiles upstream the runner is presented for six operating points (variable guide vane opening). It is shown that even at the design point, the tangential velocity profile significantly departs from the simplified one (free vortex distribution, i.e. $c_u \propto 1/r$) usually considered in preliminary design. This departure accentuates as the discharge decreases, while the axial velocity gradually develops a velocity deficit near the hub.

For the velocity field analysis on a section just upstream the runner blades we have developed an original technique to quantitatively describe the radial variation of both axial and tangential mean flow velocity components. An analytical representation of the tangential and axial velocity components is derived using a combination of three elementary vortices (one solid body vortex, Batchelor vortex and free vortex). The analytical expression parameters are computed using a least-squares method. It is shown that our swirling flow formulae match quite well the numerical data from the 3D flow simulation. We appreciate that this result is extremely useful for the turbine design, since it reduces the complex flow on an interface between the distributor and runner to a set of eight parameters.

The swirling flow number is shown to vary quasi-linearly with the guide vane opening in the

investigated operating range even if the velocity profiles are changed significantly.

Acknowledgments

The authors acknowledge the support from the National University Research Council grants (CNCSIS A Consortium 33/2006). All numerical computations have been performed at the Numerical Simulation and Parallel Computing Laboratory of the "Politehnica" University of Timisoara, National Center for Engineering of Systems with Complex Fluids.

References

Ref 1 Anton I., Hydraulic turbines, Facla Publishing House, Timisoara, Romania, 1979. (in Romanian).

Ref 2 Radha Krishna, H.C., (Editor), Hydraulic Design of Hydraulic Machinery, Avebury Publishing House, 1997.

Ref 3 Peng, G., "A Practical Combined Computation Method of Mean Through-Flow for 3D Inverse Design of Hydraulic Turbomachinery Blades", J. Fluids Eng., Vol. 127, pp. 1183-1190, 2005.

Ref 4 Bartholomä, K., "Experimentelle und Theorethische Verlustanalysein einer Kaplan Vollspiralturbine", PhD Thesis Technische Universität München, Munich, Germany, 1997.

Ref 5 Nilsson, H., "A Numerical Investigation of the turbulent Flow in a Kaplan Water Turbine Runner", PhD Thesis Chalmers University of Technology, Göteborg, Sweden, 2002.

Ref 6 Muntean, S., Balint, D., Susan-Resiga, R., Anton, I., and Darzan, C., "3D Flow Analysis in the Spiral Case and Distributor of a Kaplan Turbine", Proceedings 22nd IAHR Symposium of the Section on Hydraulic Machinery, Equipment and Cavitation, Stockholm, Sweden, paper A10-2, pp. 1-10, 2004.

Ref 7 Fluent Inc., FLUENT 6. User's Guide, Fluent Incorporated, Lebanon USA, 2001.

Ref 8 International Electrotechnical Commision, "Hydraulic Turbines, Storage, Pumps and Pumps-Turbines-Model Acceptance Tests", International Standards IEC 60193, 1999. (2nd ed.)

Ref 9 Fluent Inc., Gambit 2. User's Guide, Fluent Incorporated, Lebanon USA, 2001.

Ref 10 Balint, D., Muntean, S., and Susan-Resiga, R., "Accurate evaluation of Kaplan turbine efficiency by improving the subdomain numerical coupling approach", Proceedings of International Conference "Energy and Environment", Bucharest, Romania, 2005. (on CD-ROM)

Ref 11 Muntean, S., "Numerical methods for the analysis of the 3D flow in Francis turbine runners", PhD Thesis Politehnica University of Timisoara, Timisoara, Romania, 2002. (in Romanian)

Ref 12 Dahlhaug, O.G., "A study of swirling flow in draft tube", PhD Thesis Norwegian University of Science and Technology, Trondheim, Norway, 1997.

Ref 13 Susan-Resiga, R., Ciocan G.D., Anton, I., and Avellan, F., "Analysis of the Swirling Flow Downstream a Francis Turbine Runner", J. Fluids Eng., Vol. 128(1), pp. 177-189, 2006.

Ref 14 Batchelor, G.K., "Axial flow in trailing line vortices", J. Fluid Mech., Vol. 20, pp. 645-658, 1964.

Ref 15 Mattner, T.W., Joubert, P.N., and Chong, M.S., "Vortical flow. Part 1: Flow through a constant diameter pipe", J. Fluid Mech., Vol. 463, pp. 259-291, 2002.

Ref 16 Faler, J.H., Leibovich, S., "Disrupted states of vortex break flow and vortex breakdown", Phys. Fluids, Vol. 20(9), pp. 1385-1400, 1977.